JOURNAL OF MOLECULAR SPECTROSCOPY 168, 416–428 (1994)

Sub-Doppler Frequency Measurements on OCS at 87 THz (3.4 μm) with the CO Overtone Laser

A. DAX,*[,1] J. S. WELLS,* L. HOLLBERG,* A. G. MAKI,*[,2] AND W. URBAN†

*Time and Frequency Division, National Institute of Standards and Technology, Boulder, Colorado 80303; and †Institut für Angewandte Physik der Universität Bonn, Bonn, D-53115 Germany

Sub-Doppler frequency measurements have been made on three transitions of OCS in the 87-THz region (near 2900 cm^{-1}). The CO overtone laser was used as the saturating laser. Polarization spectroscopic techniques utilizing optical heterodyne detection were used to observe the features and subsequently provide the discriminant for locking the overtone laser to the OCS transitions. A CO_2 laser synthesizer was used to measure the frequency of the CO overtone laser and thereby measure the frequencies of the OCS lines. The resulting frequencies of the three new measurements are: 10^01–00^00 $P(27)$, 87 117 278.496(50) MHz; $11^{1f}1$–$01^{1f}0$ $R(14)$, 87 222 001.143(70) MHz for OCS; and for the $OC^{34}S$ 10^01–00^00 $P(9)$, 87 010 586.667(75) MHz, where the numbers in parentheses are the uncertainties in the last digits. These new numbers have been fitted along with more than 5700 other data points in our OCS data bank and improved constants have been obtained. These latest constants are used to calculate updated calibration tables containing values with much smaller uncertainties; three such tables are included.

INTRODUCTION

The wide acceptance of the tunable diode laser (TDL) by the spectroscopic community in the late 1970s pointed to the need for frequency calibration standards to achieve the full potential of these devices. Since 1979, we have been involved in a major effort to provide frequency/wavenumber calibration standards based on heterodyne frequency measurements (*1, 2*).

Our heterodyne frequency measurement activity came to a temporary halt when we reached the 61.76-THz (2060-cm^{-1}) region, the upper limit of our $\Delta v = 1$ CO laser (*3*). Some measurements at slightly higher frequencies were possible based on a doubling of the CO_2 laser (*4*). It was the development of the DC discharge overtone CO laser at the Institut für Angewandte Physik (IAP) in Bonn [W. Urban and coworkers (*5*)] that made further progress possible. The most recent reports (*6, 7*) suggest the potential usefulness of this laser with over 330 transitions observed in the 2.6 to 4.1 μm region. A long standing NIST–IAP collaboration was renewed in Bonn, where TDL-based heterodyne measurements were made on some OCS features in the $11^{1e}1$–$01^{1e}0$ and $11^{1f}1$–$01^{1f}0$ bands at 87 THz (3.4 μm) (*8*). Between 1979 and 1990, our measurements were all Doppler-limited with the exception of some measurements on CO (*9*) and N_2O (*10*). In a separate effort, Fayt *et al.* (*11*) have made sub-Doppler measurements on those OCS transitions that are near the 9-μm CO_2 laser transitions.

These mostly Doppler-limited frequency measurements formed the foundation for the publication of a calibration atlas (*2*) which spans much of the region from 486 to 3120 cm^{-1} plus another small region (4071–4352 cm^{-1}). The atlas has a spectral map

[1] Guest researcher from Institut für Angewandte Physik der Universität Bonn, Bonn, D-53115 Germany.
[2] Address: 15012 24th Ave. SE, Mill Creek, WA 98012.

0022-2852/94 $6.00

and facing table format which we intend to update from time to time. Since a deliberate effort was made to keep the atlas at a manageable length, about three-quarters of the possible frequency entries were not included. The diskette in NIST Standard Reference Database 39 includes these omitted values (*12*). These calibration data will also be available next year in the over the world wide electronic network.

In order to further improve the atlas, more accurate frequency measurements are required. Consequently, we have begun sub-Doppler frequency measurements at 3.4 μm. Our initial emphasis was on OCS, and we hope to include N_2O later. Our colleagues in Bonn have also made sub-Doppler frequency measurements on OCS near 5 μm (*13*). Both this paper and Ref. (*14*) describe our first OCS sub-Doppler experiments and results at NIST.

SUB-DOPPLER EXPERIMENTS WITH THE CO OVERTONE LASER

Two different experimental approaches were investigated in order to find the technique that is best suited to making measurements of OCS transitions near 3.4 μm. The first involved a normal saturated-absorption technique (*15–23*), which is much simpler to use and is potentially more accurate for frequency measurements (*17*) (provided that the transition moment of the molecule is sufficiently large). The second technique used polarization-selective optical saturation techniques (*24–35*) and produced a much better signal-to-noise ratio (SNR). However, it was considerably more cumbersome. For clarity concerning sub-Doppler spectroscopy and frequency measurements at 3 μm with a CO overtone laser, we discuss elsewhere (*14*) both types of experiments showing the advantages, limitations, and additional details of each. Because of the weak transition moment involved and some technical problems in obtaining a clean modulation signal for third-derivative detection (*21, 22*), the saturated-absorption technique was shelved for the time being.

In our NIST laboratory, we have developed a CO overtone laser similar to the one developed in Bonn (*5*). Our 1.87-m-long laser has a 450 line/mm grating and a 10 m radius output coupler. The LN_2-cooled gain section is about 1.09 m long, and the bore i.d. is 12 mm. The operating partial pressures of the He, N_2, air, and CO are essentially the same as the Bonn papers indicate. (We can attest to the wisdom of using an aluminum storage cylinder for the CO to avoid problems (*6, 7*) arising from $Fe(CO)_5$ in older iron cylinders.) The Bonn versions employ coupling from the laser utilizing the zero-order output of the grating. We chose to take the output from a dielectric coated ZnSe coupler. This compensated coupler (the second surface of the coupler is curved) minimizes the spreading of the output beam. In an effort to minimize the laser linewidth, we have inserted convection barriers to enclose the air path between the resonator optical elements and the Brewster windows of the gain tube. We have also inserted a surge reservoir between the mixing valves and the gas inlet to the laser tube to reduce pressure fluctuations caused by the flow meters.

CONSIDERATIONS OF OPTICAL HETERODYNE POLARIZATION SPECTROSCOPY

The polarization spectroscopy method was invented by Wieman and Hänsch (*24*) in 1976 for making sub-Doppler measurements. Since then, this versatile method has been used not only for several laser spectroscopic measurements, but also for laser stabilization (*25–33, 35*). The principle of operation is that a strong pump beam introduces an anisotropy in a sample; that is, the sample becomes dichroic and birefringent if the pump frequency is near a molecular resonance. A weak probe beam at

the same frequency will suffer a change in its polarization if it interacts with the same molecules as the pump beam. By use of an appropriate selection method, we can observe this change in polarization at the low power levels necessary to avoid saturating the detector. The possible variations concerning the polarization of the pump and probe and the offset angle of the analyzer from a predetermined orientation produce different signal shapes and intensities for molecular Q, R, and P transitions (*24–30*).

Because of the problems with the saturated absorption technique, we selected the optical heterodyne polarization spectroscopy technique (*20, 24, 30*). Its physical principle is extensively explained in (*31*). The main advantage of this technique is that a weak signal can be considerably enhanced by heterodyning the signal wave (amplitude E_s) with a much stronger local oscillator wave (amplitude E_0), as long as E_0 (which can also contribute noise) is selected appropriately. To use this technique, we apply an intensity modulation to the pump beam and detect the modulation transfer to the probe beam. The result is a low-noise dispersion-shaped signal which can be symmetric about the molecular transition. The J-dependence of similar dispersion signals is calculated in Refs. (*20, 24, 27, 30*).

Since both birefringence and dichroism can contribute to the signal here, the most difficult problem is to obtain a line shape that is symmetric about the true line center (*24, 32, 33*). The local oscillator wave E_0 can be obtained most conveniently from the probe beam itself by slightly uncrossing the analyzer with respect to the polarizer by an angle ϕ. An improper choice of ϕ may be accompanied by asymmetries in the dispersion signal.

Excluding noise sources originating from the environment between the laser and detector for a moment, the SNR for this type of experiment increases as $1/\sqrt{\xi}$, where ξ is the extinction ratio of the analyzer (*20, 24*). This is limited by the laser power noise γP_0 (where P_0 is the laser output power) and the detector noise D_r. One can show (*14, 34*) that for $\gamma P_0 \xi \ll D_r$,

$$\mathrm{SNR}_{\max} = \text{const.} \sqrt{\frac{P_0}{\gamma D_r}}. \tag{1}$$

A small extinction ratio of the analyzer is essential for a good signal-to-noise ratio. In the visible spectral region, extinction ratios of 10^{-7} are often cited (*24, 35*). Our Rochon-type analyzer had a theoretical extinction ratio of $\xi = 10^{-5}$ (*36*). In practice it is not quite that good, depending on the optical beam path through the crystal. By using a two-stage analyzer, we have improved the extinction ratio considerably.

By using the Jones formalism (*37*) we have calculated the contributions to the detector response I_{det} and find, by using linear approximations,

$$\begin{aligned} I_{\mathrm{det}} = Ce^{-\kappa k_0 L} E_0^2 \{ & \xi_1 \xi_2 - \xi_1 \epsilon^2 - \xi_2 \epsilon^2 + \epsilon^2 - \epsilon k_0 \Delta b_i + \phi_1^2 + \phi_1 k_0 \Delta b_r \\ & - \epsilon \Delta\kappa k_0 L + \phi_1 \Delta n k_0 L + \tfrac{1}{2}[k_0^2 \Delta n L \Delta b_r + k_0^2 \Delta\kappa L \Delta b_i] \\ & + \tfrac{1}{4}[(k_0 \Delta n L)^2 + (k_0 \Delta b_r)^2 + (\Delta\kappa k_0 L)^2 + (k_0 \Delta b_i)^2] \}, \end{aligned} \tag{2}$$

where C is a proportionality constant, κ is the susceptibility ($\kappa = \kappa_+ + \kappa_-$), $k_0 = 2\pi/\lambda$, λ is the wavelength of the probe beam, and L is the estimated overlap length of the crossed beams within the cell. The symbols ξ_1 and ξ_2 represent the extinction ratios for the first and second analyzer, respectively, ϵ is the ellipticity of the polarization after the polarizer, and $\Delta\kappa = \kappa_+ - \kappa_-$ and $\Delta n = n_+ - n_-$ are the susceptibility change and refractive index change of the anisotropic medium in the circular basis, respectively.

$\Delta\kappa$ describes the dichroism and has a Lorentzian lineshape; Δn describes the birefringence and has a dispersion lineshape; ϕ_1 is the deviation from the crossing angle of the first analyzer; and $\Delta b_r = b_r^+ - b_r^-$ (the real part) and $\Delta b_i = b_i^+ - b_i^-$ (the imaginary part) describe the anisotropy of the cell windows under vacuum stress (*20, 21, 30*).

Since both extinction ratios have similar values between 10^{-4} and 10^{-5}, the term $\xi_1\xi_2$ is negligible. The same is usually true for all terms containing ϵ^2 since we have found experimentally that $\epsilon < 10^{-3}$. The signal term can be expressed as $\phi_1 E_0(E_0\Delta n k_0 L)$, showing the heterodyning of the signal amplitude $E_0\Delta n k_0 L$ and the local oscillator amplitude $\phi_1 E_0$ (*31*). The terms $\Delta\kappa$, $(\Delta\kappa)^2$, and $(\Delta n)^2$ may lead to asymmetry of the signal, and the remaining terms are responsible for the background.

EXPERIMENTAL DETAILS

The overtone laser is the starting point of our description of the block diagram in Fig. 1. The output of the overtone laser was directed by several mirrors to a wedged uncoated ZnSe beam splitter where the transmitted portion was used for the saturating beam. The beam reflected from the front surface was used for the linear probe beam, and the beam reflected from the back surface was directed through an acousto-optic modulator to the IR frequency synthesizer. Even if the frequencies of the CO laser and the OCS line did not overlap, it was sometimes possible to shift the laser to the required frequency by placing the acousto-optic modulator (AOM) in the laser beam before it reached the beam splitter.

As indicated in Fig. 1, the probe beam's polarization was rotated by $\pi/2$ by the five-mirror variable rotator and was then focused by mirror 1 onto a reflecting wedged germanium plate polarizer (*23, 38*). The beam was recollimated by mirror 2. This increased the polarization purity of the beam from 2000:1 at the laser output to greater than 650 000:1. A four-mirror polarization conserving half-wave plate (*23, 39*) returned the polarization back to horizontal. The probe beam traversed the OCS cell at a small angle with respect to the cell axis and was focused by mirror 3 onto a second reflecting wedged germanium plate polarizer which acted as the first stage of the analyzer. Only the component polarized perpendicular to the plane of incidence was reflected by this L unit along the detection path. The local oscillator wave was generated by tilting the base of this device to the offset angle ϕ_1. A similar one-stage analyzer can also be found in Refs. (*25, 34*). These collinear signal and local oscillator beams were focused on the Rochon analyzer by mirror 4 and mirror 5 focused them on the detector.

Before considering the path of the pump beam, we point out that instead of the usual $\lambda/4$ plate, we have used a two-component scheme to achieve circular polarization. Our two-component scheme has three advantages. First, and most important, it is possible to have some control over the degree of polarization (similar to using a Babinet Soleil compensator); second, it is nearly wavelength-independent; and, third, the device is purely reflective.

The path (shown in Fig. 1) of the saturating beam through our two-component device starts where it emerges from the ZnSe beam splitter. The beam then had its polarization rotated by a three-mirror variable polarization rotator (*40*) to some arbitrary value, say Φ (the difference between a three-mirror rotator and a five-mirror rotator is that the latter conserves the polarization quality much better (*23*)). The beam was focused by mirror 6 onto a titanium plate, which affords an adjustable angle Θ of incidence relative to the incoming beam. The physics involved in the phase shift on reflection from the titanium plate is described in (*23*) and is more or less simply the physics of Fresnel reflection on a metal surface (*41*). A measured polarization

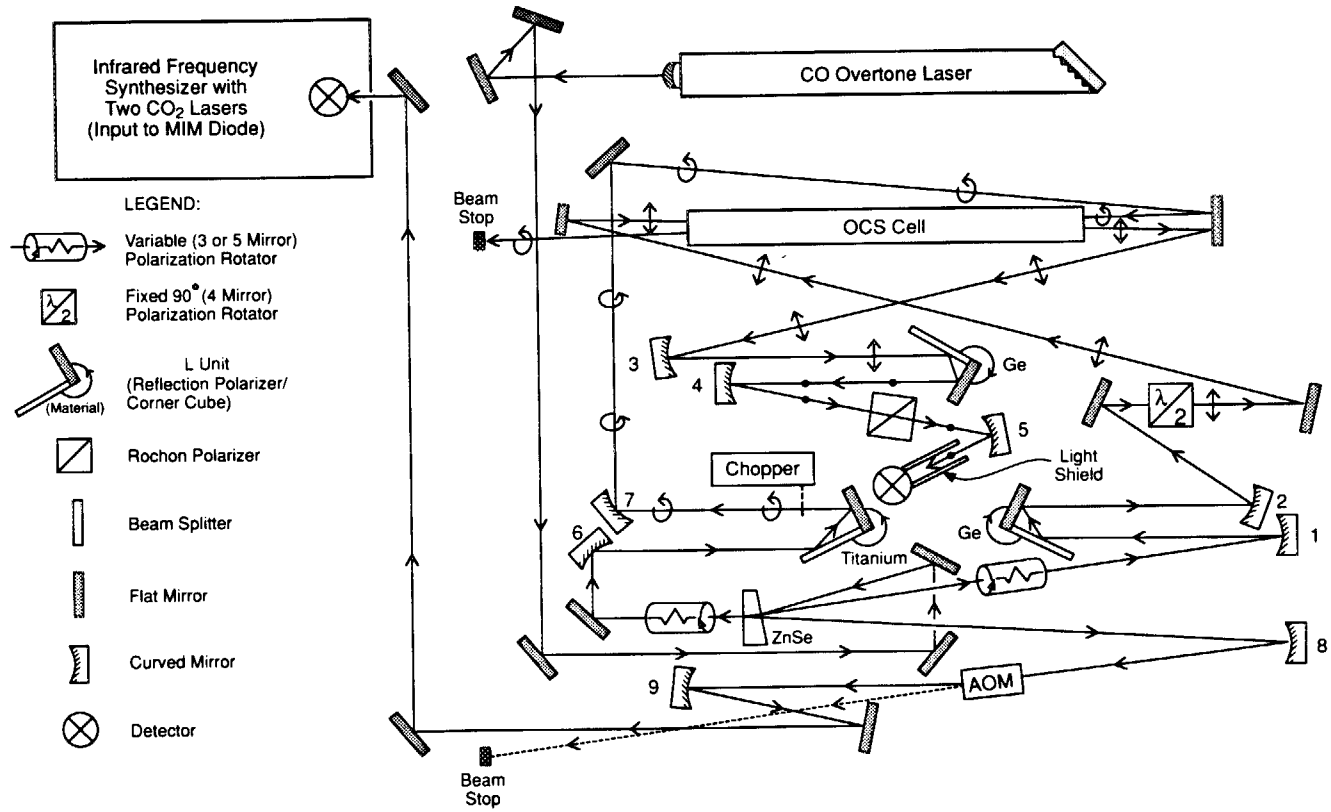

FIG. 1. Functional diagram for the sub-Doppler frequency measurement of the $P(27)$ line in the OCS 10^01–00^00 band at 3.4 μm.

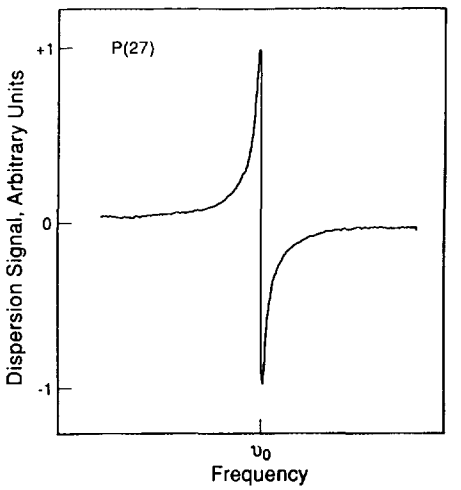

FIG. 2. Dispersion signal of the saturated $P(27)$ transition. The center frequency is 87 117 278.496(50) MHz and the peak to peak linewidth is about 700 kHz. The width of the scan shown here is about 45 MHz.

quality of 99.5% was achieved for the saturation beam by iterative adjustment of the angles, Φ and Θ. It is essential to have a good circular polarization quality here; otherwise, the pump wave can be considered to be composed of a circular and a linear part where dichroism can be accompanied with this linear pump wave. According to Ref. (*25*), such a dichroism changes the azimuth angle of the probe beam's linear polarization. This, in turn, increases the Lorentzian shaped contribution to the signal thus giving greater asymmetry to the detected dispersion signal. The saturation beam traversed the cell at a small angle with the cell axis. The crossing angle between the two beams was estimated to be about 1 mrad.

The elimination of stray light was tedious and is detailed in Ref. (*14*). When this was accomplished, we were able to measure three OCS transitions which had accidental overlaps with the CO overtone laser or its AOM shifted sidebands. Some of the data from the experiment on the $P(27)A$ line of OCS at 3.4 μm are shown in Figs. 2 and

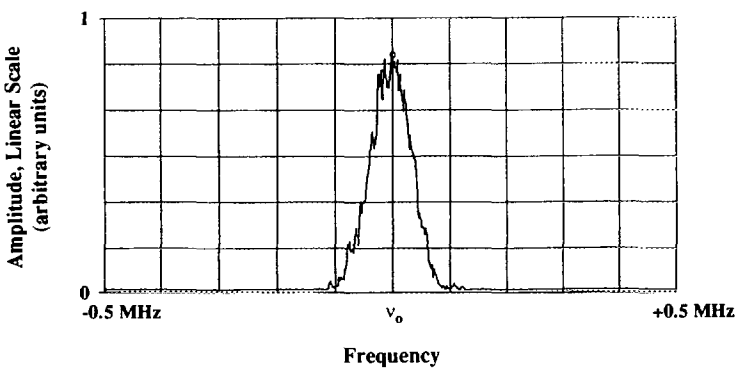

FIG. 3. Spectrum analyzer display of the time-averaged (100 scans) beatnote between the CO overtone laser which was locked to the $P(27)$ line and a reference from the infrared frequency synthesizer. The center frequency is 1171.900 MHz, the video bandwidth is 30 kHz, and the sweep time is 62.56 msec.

3. Figure 2 shows the dispersion signal which was used to lock the CO overtone laser. The signal appears fairly symmetric.

In order to obtain a symmetric lineshape, we rotated the second analyzer (Rochon crystal) of our two-stage system relative to the first analyzer. Offset angles of $\phi_2 < 5°$ were enough to achieve symmetric signals. Since the polarization of the probe beam after the first analyzer is elliptical, this technique bears some resemblance to the method employed by Delsard and Keller (*26*). They used a linear pump beam and a circular probe beam, and found that it was possible to change the signal continuously from an absorption shape to a dispersion shape simply by rotating their analyzer 45°.

Our quantitative description does not demonstrate that we can symmetrize the signal without changing the real zero-crossing of the Lamb dip. To do this would require the inclusion of a valid model which describes the cell windows under stress as well as our offset angle ϕ_2. However, not only do the dispersion signals appear symmetric, but also another measurement using a different technique produced a result which agreed to within 20 kHz with our result for the same 5.3-μm OCS transition (*13, 42*).

Referring again to Fig. 1, the third beam from our wedged ZnSe beamsplitter was focused by mirror 8 on the AOM, and the shifted beam was recollimated and sent to the input of the infrared frequency synthesizer. The frequency synthesizer consists of two CO_2 laser frequency standards, a microwave oscillator, a MIM diode, and a spectrum analyzer along with a marker oscillator. (See Ref. (*2*), pp. 17–21, or Refs. (*3, 4, 8*).) Reference (*14*) contains details of the latest improvements of the CO_2 laser systems.

Figure 3 shows the time averaged beatnote between the locked CO overtone laser and a reference synthesized from a combination of two CO_2-stabilized laser standards. Aside from the frequency, which is the primary goal, two features are significant. The first is that the linewidth of the laser is about 100 kHz, which is considerably less than the 700-kHz saturation feature. The relative phase and amplitudes of modulation of the reference lasers were adjusted to minimize the beatnote linewidth; hence, the linewidth here is an upper limit on that of the CO laser. The second feature (not discernible here) is the SNR of the beatnote which was generally observed to be between 25 and 30 dB, and hence suitable for stabilizing the overtone laser to the synthesized reference. This makes it an ideal reference for use in a heterodyne measurement to measure the linewidth of TDLs and to use in frequency offset control in an alternate scheme with a line-narrowed TDL (*43*).

Dispersion signals similar to that in Fig. 2 were obtained for two other transitions. These measurements were made at pressures of about 1.3 Pa (10 mTorr) with an estimated overlap pathlength of about 1 m in a 1.5-m-long absorption cell. The measurements were all made with the same sample of gas at room temperature. No isotopically enriched samples (^{34}S for example) were used in the measurements.

RESULTS AND ANALYSIS

Table I gives the three saturated-absorption frequency measurements made through the use of this polarization spectroscopic technique. Of course, this technique is limited to the measurement of transitions that are within the small tuning range of the CO laser lines, or within the range of the sideband produced by the acousto-optic modulator.

The CO_2 laser frequencies used to calculate the observed frequencies given in Table I were taken from a recent reanalysis of the CO_2 laser frequencies (*44*) and, for the lines used for this work, only differ from the frequencies given by Bradley *et al.* (*45*)

TABLE I

The Measured Transition Frequencies for Carbonyl Sulfide

CO Trans.[a]	OCS Transition		Obs. Freq.[b] (MHz)	CO_2 Freq. Stds.[c]	Beat Freq. (MHz)
$P_{26}(9)$	$P(27)$	10^01-00^00	87 117 278.496±0.050	$2\times R(8)\mathrm{I}+R(12)\mathrm{I}$	-1261.908
$P_{26}(8)$	$R(14)$	$11^{1f}1-01^{1f}0$	87 222 001.143±0.070	$2\times P(28)\mathrm{I}+P(32)\mathrm{II}$	-1056.507[d]
$P_{26}(10)$	$P(9)$[e]	10^01-00^00	87 010 586.667±0.075	$2\times R(28)\mathrm{I}+P(24)\mathrm{I}$	-412.438

[a] For the CO laser designation the subscript indicates the lower state vibrational quantum number and the number in parentheses is J''.
[b] The OCS observed frequency is given by the sum of the CO_2 laser frequencies and the beat frequency.
[c] For the CO_2 laser designation the I indicates the 10 μm band and the II indicates the 9 μm band.
[d] For the measurement of the $R(14)$ line of the $11^{1f}1-01^{1f}0$ band a microwave frequency of 10 999.988 MHz was added to the CO_2 laser frequencies.
[e] This transition is for $^{16}O^{12}C^{34}S$; the other two are for $^{16}O^{12}C^{32}S$.

by a few kilohertz. The uncertainties in the measurements were about 30 kHz for the absolute frequencies of the synthesized references, or about 10 kHz for each of the three CO_2 laser harmonics. The remaining contribution to the uncertainty was that due to locating the line center. This depended on the ratio of asymmetry of the dispersion signal to the signal amplitude with an additional contribution due to the noise.

These measurements have been combined in a least-squares fit with the many other measurements on OCS that were used in Ref. (*2*). In addition, some more recent FTS

TABLE II

The Rovibrational Constants (in cm^{-1}) Used to Fit the Data

State	B_v	$D_v\times10^8$	$H_v\times10^{14}$	$L_v\times10^{17}$
$^{16}O^{12}C^{32}S$				
00^00	0.202 856 740 854(398)[a]	4.340 677 1(1187)	−0.326 19(1452)	
01^10	0.203 209 834 843(1006)	4.411 511 2(1497)	−0.256 97(1803)	
10^01	0.201 103 238 50(5499)	5.137 499(5107)	86.768(2420)	−7.921 2(5145)[b]
11^11	0.201 516 185 28(6599)	4.774 825(3871)	13.797 9(8046)	−0.429 90(5429)
$^{16}O^{12}C^{34}S$				
00^00	0.197 898 035 007(3272)	4.141 187 4(6101)	−0.351 71(8951)	
10^01	0.196 197 685 12(10560)	5.000 256(7002)	68.962(1599)	−2.680 3(1161)

State	$q_v\times10^4$	$q_{vJ}\times10^{10}$	$q_{vJJ}\times10^{14}$
$^{16}O^{12}C^{32}S$			
01^10	2.121 938 676(253)	1.424 123(492)	0.057 395(2118)
11^11	2.377 549(462)	10.916 3(2087)	3.090 4(2204)

	Vib. Transition	ν_0
$^{16}O^{12}C^{32}S$		
	10^01-00^00	2918.105 066 6(248)
	11^11-01^10	2903.717 546 5(144)
$^{16}O^{12}C^{34}S$		
	10^01-00^00	2906.045 274 8(75)

[a] The estimated uncertainty (one standard deviation) in the last digits is given in parentheses.
[b] The fit of the 10^01 level of $^{16}O^{12}C^{32}S$ also included $M_v = 4.467(\pm0.484)\times10^{-21}$ cm^{-1} and $N_v = -1.110(\pm0.166)\times10^{-25}$ cm^{-1}.

measurements were included in the fit in such a way as to allow the heterodyne measurements to determine the vibrational energy levels. The FTS measurements were necessary to determine the values of the higher order vibrational terms, i.e., the L_v terms. Table II shows the vibrational constants that resulted from this fit. Enough digits are given for the constants to allow for correlation among the constants and to ensure that the observed frequencies (actually their deviations) are correctly calculated.

The least-squares analysis made use of the term equations

$$E_v = G_v + B_v J(J+1) - D_v[J(J+1) - l^2]^2 + H_v[J(J+1) - l^2]^3 + L_v[J(J+1) - l^2]^4 + M_v[J(J+1) - l^2]^5 + N_v[J(J+1) - l^2]^6 \quad (3)$$

and

$$\nu_0 = G'_v - G''_v. \quad (4)$$

TABLE III

Wavenumbers (cm^{-1}) Calculated for the 10^01–00^00 Band of $^{16}O^{12}C^{32}S$

P-Branch	*J*"	*R*-Branch	*P*-Branch	*J*"	*R*-Branch
...	0	2918.507 273 (49)[a]	2898.038 623 (32)	42	2932.195 776 (34)
2917.699 353 (50)	1	2918.905 971 (49)	2897.484 749 (33)	43	2932.444 165 (35)
2917.290 134 (49)	2	2919.301 159 (48)	2896.927 304 (34)	44	2932.688 887 (36)
2916.877 410 (49)	3	2919.692 836 (48)	2896.366 284 (35)	45	2932.929 936 (37)
2916.461 181 (48)	4	2920.081 000 (47)	2895.801 689 (36)	46	2933.167 308 (38)
2916.041 448 (48)	5	2920.465 649 (46)	2895.233 517 (37)	47	2933.401 000 (38)
2915.618 211 (47)	6	2920.846 780 (44)	2894.661 765 (37)	48	2933.631 009 (39)
2915.191 471 (46)	7	2921.224 392 (43)	2894.086 432 (38)	49	2933.857 330 (40)
2914.761 227 (44)	8	2921.598 482 (41)	2893.507 516 (39)	50	2934.079 960 (42)
2914.327 479 (43)	9	2921.969 047 (39)	2892.925 016 (40)	51	2934.298 895 (44)
2913.890 226 (41)	10	2922.336 085 (37)	2892.338 931 (42)	52	2934.514 131 (46)
2913.449 469 (39)	11	2922.699 591 (35)	2891.749 257 (44)	53	2934.725 666 (48)
2913.005 206 (37)	12	2923.059 564 (33)	2891.155 995 (46)	54	2934.933 496 (51)
2912.557 436 (35)	13	2923.416 000 (31)	2890.559 143 (48)	55	2935.137 617 (55)
2912.106 158 (33)	14	2923.768 895 (29)	2889.958 699 (51)	56	2935.338 027 (58)
2911.651 371 (31)	15	2924.118 246 (26)	2889.354 663 (55)	57	2935.534 721 (62)
2911.193 074 (29)	16	2924.464 049 (24)	2888.747 032 (58)	58	2935.727 697 (66)
2910.731 265 (26)	17	2924.806 301 (21)	2888.135 807 (62)	59	2935.916 952 (71)
2910.265 943 (24)	18	2925.144 996 (19)	2887.520 985 (66)	60	2936.102 482 (75)
2909.797 105 (21)	19	2925.480 133 (16)	2886.902 566 (71)	61	2936.284 285 (79)
2909.324 751 (19)	20	2925.811 705 (14)	2886.280 549 (75)	62	2936.462 357 (83)
2908.848 877 (16)	21	2926.139 710 (11)	2885.654 932 (79)	63	2936.636 695 (88)
2908.369 482 (14)	22	2926.464 142 (09)	2885.025 716 (83)	64	2936.807 297 (91)
2907.886 565 (11)	23	2926.784 998 (06)	2884.392 898 (88)	65	2936.974 159 (95)
2907.400 122 (09)	24	2927.102 273 (04)	2883.756 478 (91)	66	2937.137 279 (98)
2906.910 151 (06)	25	2927.415 963 (03)	2883.116 455 (95)	67	2937.296 65 (10)
2906.416 650 (04)	26	2927.726 062 (04)	2882.472 829 (98)	68	2937.452 28 (10)
2905.919 618 (03)	27	2928.032 568 (06)	2881.825 60 (10)	69	2937.604 16 (11)
2905.419 051 (04)	28	2928.335 475 (08)	2881.174 76 (10)	70	2937.752 28 (11)
2904.914 946 (06)	29	2928.634 778 (11)	2880.520 32 (11)	71	2937.896 64 (11)
2904.407 303 (08)	30	2928.930 474 (13)	2879.862 27 (11)	72	2938.037 25 (11)
2903.896 117 (11)	31	2929.222 557 (16)	2879.200 62 (11)	73	2938.174 10 (11)
2903.381 387 (13)	32	2929.511 023 (18)	2878.535 35 (11)	74	2938.307 17 (11)
2902.863 111 (16)	33	2929.795 867 (20)	2877.866 48 (11)	75	2938.436 49 (11)
2902.341 285 (18)	34	2930.077 086 (22)	2877.194 00 (11)	76	2938.562 03 (11)
2901.815 908 (20)	35	2930.354 674 (24)	2876.517 91 (11)	77	2938.683 81 (11)
2901.286 976 (22)	36	2930.628 628 (26)	2875.838 22 (11)	78	2938.801 81 (11)
2900.754 488 (24)	37	2930.898 942 (28)	2875.154 91 (11)	79	2938.916 03 (11)
2900.218 442 (26)	38	2931.165 613 (30)	2874.467 99 (11)	80	2939.026 47 (11)
2899.678 834 (28)	39	2931.428 636 (31)	2873.777 46 (11)	81	2939.133 14 (11)
2899.135 663 (30)	40	2931.688 007 (32)	2873.083 32 (11)	82	2939.236 02 (11)
2898.588 927 (31)	41	2931.943 721 (33)	2872.385 57 (11)	83	2939.335 11 (11)

[a] The estimated uncertainty in the last digits (twice the standard deviation) is given in parentheses.

TABLE IV

Wavenumbers (cm^{-1}) Calculated for the $11^{1}1$–$01^{1}0$ Band of $^{16}O^{12}C^{32}S$

P-Branch	*J*"	*R*-Branch	*P*-Branch	*J*"	*R*-Branch
...	1	2904.520 724 (28)	2883.746 229 (61)	42	2917.994 773 (61)
2902.900 922 (28)	2	2904.917 267 (27)	2883.198 259 (61)	43	2918.251 229 (61)
2902.487 570 (28)	3	2905.310 444 (26)	2882.646 898 (61)	44	2918.504 195 (62)
2902.070 859 (27)	4	2905.700 255 (25)	2882.092 144 (61)	45	2918.753 668 (62)
2901.650 790 (26)	5	2906.086 697 (23)	2881.533 995 (62)	46	2918.999 643 (62)
2901.227 363 (25)	6	2906.469 769 (21)	2880.972 448 (62)	47	2919.242 116 (62)
2900.800 579 (23)	7	2906.849 469 (19)	2880.407 503 (62)	48	2919.481 083 (62)
2900.370 440 (21)	8	2907.225 795 (17)	2879.839 156 (62)	49	2919.716 541 (62)
2899.936 944 (19)	9	2907.598 746 (15)	2879.267 407 (62)	50	2919.948 484 (62)
2899.500 092 (17)	10	2907.968 319 (12)	2878.692 252 (62)	51	2920.176 909 (62)
2899.059 885 (15)	11	2908.334 512 (10)	2878.113 691 (62)	52	2920.401 811 (63)
2898.616 322 (12)	12	2908.697 323 (07)	2877.531 721 (62)	53	2920.623 188 (63)
2898.169 404 (10)	13	2909.056 749 (05)	2876.946 339 (63)	54	2920.841 033 (64)
2897.719 131 (07)	14	2909.412 789 (04)	2876.357 545 (63)	55	2921.055 344 (64)
2897.265 502 (05)	15	2909.765 440 (05)	2875.765 336 (64)	56	2921.266 116 (65)
2896.808 517 (04)	16	2910.114 699 (08)	2875.169 711 (64)	57	2921.473 346 (66)
2896.348 175 (05)	17	2910.460 563 (11)	2874.570 666 (65)	58	2921.677 028 (67)
2895.884 477 (08)	18	2910.803 031 (14)	2873.968 201 (66)	59	2921.877 160 (68)
2895.417 421 (11)	19	2911.142 098 (17)	2873.362 313 (67)	60	2922.073 736 (69)
2894.947 007 (14)	20	2911.477 763 (20)	2872.753 000 (68)	61	2922.266 753 (70)
2894.473 235 (17)	21	2911.810 021 (23)	2872.140 260 (69)	62	2922.456 207 (71)
2893.996 104 (20)	22	2912.138 871 (27)	2871.524 092 (70)	63	2922.642 094 (72)
2893.515 612 (23)	23	2912.464 309 (30)	2870.904 494 (71)	64	2922.824 410 (73)
2893.031 759 (27)	24	2912.786 332 (33)	2870.281 463 (72)	65	2923.003 150 (75)
2892.544 544 (30)	25	2913.104 936 (36)	2869.654 998 (73)	66	2923.178 312 (76)
2892.053 966 (33)	26	2913.420 119 (39)	2869.025 097 (75)	67	2923.349 889 (77)
2891.560 024 (36)	27	2913.731 877 (41)	2868.391 757 (76)	68	2923.517 880 (78)
2891.062 716 (39)	28	2914.040 206 (44)	2867.754 978 (77)	69	2923.682 279 (80)
2890.562 041 (41)	29	2914.345 103 (46)	2867.114 757 (78)	70	2923.843 084 (81)
2890.057 999 (44)	30	2914.646 564 (48)	2866.471 092 (80)	71	2924.000 289 (81)
2889.550 587 (46)	31	2914.944 587 (50)	2865.823 982 (81)	72	2924.153 890 (82)
2889.039 804 (48)	32	2915.239 166 (52)	2865.173 424 (81)	73	2924.303 885 (83)
2888.525 648 (50)	33	2915.530 299 (54)	2864.519 418 (82)	74	2924.450 269 (83)
2888.008 119 (52)	34	2915.817 982 (55)	2863.861 960 (83)	75	2924.593 037 (84)
2887.487 215 (54)	35	2916.102 211 (57)	2863.201 049 (83)	76	2924.732 186 (84)
2886.962 933 (55)	36	2916.382 982 (58)	2862.536 684 (84)	77	2924.867 712 (86)
2886.435 272 (57)	37	2916.660 291 (59)	2861.868 861 (84)	78	2924.999 610 (88)
2885.904 232 (58)	38	2916.934 134 (60)	2861.197 580 (86)	79	2925.127 878 (92)
2885.369 809 (59)	39	2917.204 508 (60)	2860.522 839 (88)	80	2925.252 509 (99)
2884.832 002 (60)	40	2917.471 409 (61)	2859.844 635 (92)	81	2925.373 50 (11)
2884.290 809 (60)	41	2917.734 832 (61)	2859.162 967 (99)	82	2925.490 85 (13)

[a] The estimated uncertainty in the last digits (twice the standard deviation) is given in parentheses.

In addition, for the $l = 1$ states, the l-doubling was taken into account by adding the terms

$$\pm[q_v J(J+1) - q_{vJ} J^2(J+1)^2 + q_{vJJ} J^3(J+1)^3], \tag{5}$$

where the upper sign (+) was used for the f levels and the lower sign (−) was used for the e levels.

As discussed by Maki *et al.* (*46*), there is a weak resonance between the $10^{0}1$ and $04^{0}1$ states and a similar resonance between the $11^{1}1$ and $05^{1}1$ states. This resonance has been investigated in more detail by Fayt (*47, 48*). It causes the effective values of the H_v, L_v, M_v, and N_v terms to be much larger than in the ground state; consequently, it was necessary to include those constants in the least-squares fits. Although it is surprising that an N_v term should be so large that it is needed to fit the data, the value that we find for the $10^{0}1$ state is not as large as that predicted by Fayt *et al.* (*49*) from their analysis.

TABLE V

Wavenumbers (cm^{-1}) Calculated for the $10^01–00^00$ Band of $^{16}O^{12}C^{34}S$

P-Branch	*J"*	*R*-Branch	*P*-Branch	*J"*	*R*-Branch
...	0	2906.437 670 (15)[a]	2886.483 94 (10)	42	2919.807 87 (10)
2905.649 479 (15)	1	2906.826 663 (14)	2885.944 16 (10)	43	2920.050 78 (10)
2905.250 283 (15)	2	2907.212 253 (13)	2885.400 90 (10)	44	2920.290 12 (10)
2904.847 689 (14)	3	2907.594 438 (11)	2884.854 15 (10)	45	2920.525 874 (99)
2904.441 696 (13)	4	2907.973 216 (9)	2884.303 90 (10)	46	2920.758 040 (99)
2904.032 305 (11)	5	2908.348 586 (7)	2883.750 170 (99)	47	2920.986 614 (98)
2903.619 516 (9)	6	2908.720 544 (5)	2883.192 940 (99)	48	2921.211 593 (98)
2903.203 329 (7)	7	2909.089 089 (4)	2882.632 214 (98)	49	2921.432 972 (97)
2902.783 745 (5)	8	2909.454 218 (5)	2882.067 989 (98)	50	2921.650 749 (97)
2902.360 761 (4)	9	2909.815 928 (8)	2881.500 263 (97)	51	2921.864 919 (96)
2901.934 379 (5)	10	2910.174 217 (12)	2880.929 034 (97)	52	2922.075 479 (96)
2901.504 597 (8)	11	2910.529 080 (16)	2880.354 301 (96)	53	2922.282 426 (96)
2901.071 414 (12)	12	2910.880 516 (20)	2879.776 063 (96)	54	2922.485 756 (95)
2900.634 829 (16)	13	2911.228 519 (25)	2879.194 318 (96)	55	2922.685 467 (95)
2900.194 840 (20)	14	2911.573 087 (29)	2878.609 065 (95)	56	2922.881 555 (94)
2899.751 447 (25)	15	2911.914 216 (34)	2878.020 302 (95)	57	2923.074 018 (93)
2899.304 647 (29)	16	2912.251 902 (39)	2877.428 030 (94)	58	2923.262 853 (93)
2898.854 438 (34)	17	2912.586 141 (44)	2876.832 247 (93)	59	2923.448 058 (92)
2898.400 820 (39)	18	2912.916 928 (48)	2876.232 953 (93)	60	2923.629 630 (91)
2897.943 789 (44)	19	2913.244 259 (53)	2875.630 147 (92)	61	2923.807 567 (91)
2897.483 343 (48)	20	2913.568 130 (58)	2875.023 828 (91)	62	2923.981 867 (90)
2897.019 480 (53)	21	2913.888 536 (62)	2874.413 997 (91)	63	2924.152 528 (90)
2896.552 197 (58)	22	2914.205 472 (67)	2873.800 653 (90)	64	2924.319 546 (91)
2896.081 492 (62)	23	2914.518 934 (71)	2873.183 796 (90)	65	2924.482 922 (92)
2895.607 363 (67)	24	2914.828 917 (75)	2872.563 426 (91)	66	2924.642 652 (94)
2895.129 805 (71)	25	2915.135 415 (79)	2871.939 543 (92)	67	2924.798 734 (96)
2894.648 817 (75)	26	2915.438 424 (83)	2871.312 147 (94)	68	2924.951 17 (10)
2894.164 396 (79)	27	2915.737 939 (86)	2870.681 238 (96)	69	2925.099 95 (10)
2893.676 538 (83)	28	2916.033 955 (89)	2870.046 816 (99)	70	2925.245 08 (11)
2893.185 240 (86)	29	2916.326 466 (91)	2869.408 88 (10)	71	2925.386 55 (11)
2892.690 500 (89)	30	2916.615 467 (94)	2868.767 43 (11)	72	2925.524 37 (12)
2892.192 314 (91)	31	2916.900 954 (96)	2868.122 47 (11)	73	2925.658 52 (12)
2891.690 679 (94)	32	2917.182 921 (98)	2867.474 00 (12)	74	2925.789 01 (13)
2891.185 592 (96)	33	2917.461 362 (99)	2866.822 01 (12)	75	2925.915 84 (13)
2890.677 049 (98)	34	2917.736 27 (10)	2866.166 51 (13)	76	2926.039 00 (13)
2890.165 048 (99)	35	2918.007 65 (10)	2865.507 49 (13)	77	2926.158 49 (13)
2889.649 59 (10)	36	2918.275 48 (10)	2864.844 96 (13)	78	2926.274 30 (13)
2889.130 66 (10)	37	2918.539 77 (10)	2864.178 91 (13)	79	2926.386 43 (13)
2888.608 26 (10)	38	2918.800 51 (10)	2863.509 34 (13)	80	2926.494 88 (14)
2888.082 40 (10)	39	2919.057 70 (10)	2862.836 25 (13)	81	2926.599 64 (14)
2887.553 06 (10)	40	2919.311 32 (10)	2862.159 63 (14)	82	2926.700 70 (16)
2887.020 24 (10)	41	2919.561 38 (10)	2861.479 50 (14)	83	2926.798 07 (18)

[a] The estimated uncertainty in the last digits (twice the standard deviation) is given in parentheses.

The new constants are not very different from the previously determined constants (*2, 46, 49*) because the one accurate heterodyne measurement for each vibrational transition does not change any one constant by very much, but rather changes all the constants by a small amount. However, those new constants, with the new variance-covariance matrix elements, can now be used to calculate more reliable transition frequencies and their uncertainties.

Tables III, IV, and V give new tables of OCS absorption line wavenumbers that can be used for calibration. Even though the table lists uncertainties that are twice the standard deviation, experience has shown us that they should be treated as if they were a single standard deviation. It would not be unusual if subsequent measurements of the high-J transitions changed the numbers by two or three times the uncertainty given in the table. In order to further improve the reliability of the calibration numbers for these bands, it would be useful to make at least one more sub-Doppler frequency measurement for these bands at J values that differ from the present measurements

by at least 15 units. Until more sub-Doppler measurements are made, the calculated wavenumbers for transitions with J values more than 10 units from the measured J values should be treated with skepticism.

In the least-squares fit for the most abundant isotopic species over 5700 transitions were included although many of those transitions did not involve either the upper or lower state of the transitions measured in this work. For the $OC^{34}S$ species, far fewer frequency measurements have been made, but again, all the data used in Refs. (*2, 46*) were included in the present fit along with some more recent FTS measurements.

ACKNOWLEDGMENTS

This work was supported in part by the NASA Office of Upper Atmospheric Research. The authors thank M. Winnewisser and co-workers for providing the FTS spectrum of OCS in this region. A. Dax was funded by the Deutsche Forschungsgemeinschaft and the Graduiertenkolleg "Wechselwirkung in Molekülen" in Bonn, Germany. The Institut für Angewandte Physik provided a large quantity of optics for this experiment. We thank B. Nelles and his co-workers from Carl Zeiss for polishing the Ti-mirror, and Mr. Koch from the Deutsche Titan GmbH Düsseldorf for making the substrate available to us. We also thank S. Gilbert of NIST for valuable suggestions regarding the paper.

RECEIVED: June 23, 1994

REFERENCES

1. J. S. WELLS, F. R. PETERSEN, AND A. G. MAKI, *Appl. Opt.* **18,** 3567–3573 (1979).
2. A. G. MAKI AND J. S. WELLS, "Wavenumber Calibration Tables From Heterodyne Frequency Measurements," NIST Special Publication 821, U.S. Government Printing Office, Washington, DC, 1991.
3. J. S. WELLS, M. SCHNEIDER, AND A. G. MAKI, *J. Mol. Spectrosc.* **140,** 170–176 (1990).
4. A. G. MAKI, J. S. WELLS, AND D. A. JENNINGS, *J. Mol. Spectrosc.* **144,** 224–229 (1990).
5. M. GROMOLL-BOHLE, W. BOHLE, AND W. URBAN, *Opt. Commun.* **69,** 409–413 (1989).
6. E. BACHEM, A. DAX, A. WEIDENFELLER, M. SCHNEIDER, AND W. URBAN, *Appl. Phys. B* **57,** 185–191 (1993).
7. T. GEORGE, Internal Report, Institut für Angewandte Physik, Universität Bonn, Germany, 1991. [Unpublished]
8. A. DAX, M. MÜRTZ, J. S. WELLS, M. SCHNEIDER, E. BACHEM, W. URBAN, AND A. G. MAKI, *J. Mol. Spectrosc.* **156,** 98–103 (1992).
9. C. R. POLLOCK, F. R. PETERSEN, D. A. JENNINGS, J. S. WELLS, AND A. G. MAKI, *J. Mol. Spectrosc.* **99,** 357–368 (1983).
10. C. R. POLLOCK, F. R. PETERSEN, D. A. JENNINGS, J. S. WELLS, AND A. G. MAKI, *J. Mol. Spectrosc.* **107,** 62–71 (1984).
11. A. FAYT, J. G. LAHAYE, J. LEMAIRE, F. HERLEMONT, AND J. G. BANTEGNIE, *J. Mol. Spectrosc.* **140,** 252–258 (1990).
12. A. G. MAKI AND J. S. WELLS, NIST Standard Reference Data 39. [This can be purchased from Standard Reference Data, NIST Bldg 221/Room A32, Gaithersburg, Maryland 20899, or telephoning (301) 975-2208]
13. T. GEORGE, M. H. WAPPELHORST, S. SAUPE, M. MÜRTZ, W. URBAN, AND A. G. MAKI, *J. Mol. Spectrosc.*, in press.
14. A. DAX, J. S. WELLS, L. HOLLBERG, A. G. MAKI, AND W. URBAN, NIST Tech. Note No. 1365, 1994.
15. V. P. CHEBOTAYEV, *Phys. Rep.* **119,** 75–116 (1985).
16. A. CLAIRON, O. ACEF, C. CHARDONNET, AND C. J. BORDÉ, *in* "Frequency Standards and Metrology" (A. DeMarchi, Ed.), Springer, Berlin, 1989.
17. M. D. LEVENSON, "Introduction to Nonlinear Spectroscopy", Academic Press, New York, 1982.
18. B. COUILLAUD, *in* "Progress in Atomic Spectroscopy" (W. Hanle and H. Kleinpoppen, Eds.), Part C, Plenum Press, New York, 1984.
19. MURRAY SARGENT III, *Phys. Rev. A* **14,** 524–527 (1976).
20. R. E. TEETS, F. V. KOWALSKI, W. T. HILL, N. CARLSON, AND T. W. HÄNSCH, *SPIE* **113,** 80–87 (1977).
21. W. DEMTRÖDER, *in* "Laser Spectroscopy: Basic Concepts and Instrumentation," Springer, Berlin, 1981. [See for example, pp. 494–499.]
22. F. BAYER-HELMS AND J. HELMCKE, PTB-Bericht Me-17, Braunschweig, Germany, 1977.

23. A. DAX, Ph.D. thesis, Institut für Angewandte Physik, Universität of Bonn, Germany, 1992.
24. C. WIEMAN AND T. W. HÄNSCH, *Phys. Rev. Lett.* **36,** 1170–1173 (1976).
25. V. STERT AND R. FISCHER, *Appl. Phys.* **17,** 151–154 (1978).
26. C. DELSART AND J. C. KELLER, *in* "Laser Spectroscopy III" (J. L. Hall and J. L. Carlsten, Eds.), Springer, Berlin, 1977.
27. S. SAIKAN, *J. Opt. Soc. Am.* **68,** 1184–1187 (1978).
28. D. GODDON, A. GROH, H. J. HANSES, M. SCHNEIDER, AND W. URBAN, *J. Mol. Spectrosc.* **147,** 392–397 (1991).
29. A. GROH, D. GODDON, M. SCHNEIDER, W. ZIMMERMANN, AND W. URBAN, *J. Mol. Spectrosc.* **146,** 161–168 (1991).
30. M. RAAB, G. HÖNING, W. DEMTRÖDER, AND C. R. VIDAL, *J. Chem. Phys.* **76,** 4370–4386 (1982).
31. M. D. LEVENSON AND G. L. EESLEY, *Appl. Phys.* **19,** 1–17 (1979).
32. C. WIEMAN AND T. W. HÄNSCH, *Phys. Rev. A* **22,** 192–205 (1980).
33. CH. BELFRAGE, P. GRAFSTRÖM, S. KRÖLL, AND S. SVANBERG, *Phys. Scr.* **27,** 367–370 (1983).
34. W. BOHLE, internal report, Institut für Angewandte Physik, Universität Bonn, Germany, 1989. [Unpublished]
35. M. RAAB AND A. WEBER, *J. Opt. Soc. Am. B.* **2,** 1476–1479 (1985).
36. BERNHARD HALLE NACHF. GmbH & Co., Berlin Germany, data sheet, 1991; a copy can be obtained on request to one of the authors (JSW). It is also on deposit in the Editorial Office of this journal.
37. R. M. A. AZZAM, "Ellipsometry and Polarized Light," North-Holland, Amsterdam, 1977.
38. M. V. R. K. MURTY AND R. P. SHUKLA, *Appl. Opt.* **22,** 1094–1098 (1983).
39. A. R. CHRAPLYVY, *Appl. Opt.* **15,** 2022–2023 (1976).
40. C. E. GRENIGER, *Appl. Opt.* **27,** 774–776 (1988).
41. M. BORN, "Principles of Optics," 6th ed., Pergamon Press, Oxford, 1987.
42. J. S. WELLS, A. DAX, L. HOLLBERG, AND A. G. MAKI, *J. Mol. Spectrosc.*, in press.
43. M. MÜRTZ, M. SCHAEFER, M. SCHNEIDER, J. S. WELLS, W. URBAN, U. SCHIESSL, AND M. TACKE, *Opt. Commun.* **94,** 551–556 (1992).
44. A. G. MAKI, C-C. CHOU, K. M. EVENSON, L. R. ZINK, AND J-T. SHY, *J. Mol. Spectrosc.* **167,** 211–214 (1994).
45. L. C. BRADLEY, K. L. SOOHOO, AND C. FREED, *IEEE J. Quantum Electron.* **QE-22,** 234–267 (1986).
46. A. G. MAKI, J. S. WELLS, AND J. B. BURKHOLDER, *J. Mol. Spectrosc.* **147,** 173–181 (1991).
47. A. FAYT, *Ann. Soc. Sci. Brussels* **82,** 101–112 (1968).
48. A. FAYT, *Ann. Soc. Sci. Brussels* **84,** 69–106 (1970).
49. A. FAYT, R. VANDENHAUTE, AND J. G. LAHAYE, *J. Mol. Spectrosc.* **119,** 233–266 (1986).